Article

Cell Reports

# CSNAP Is a Stoichiometric Subunit of the COP9 Signalosome

## Graphical Abstract

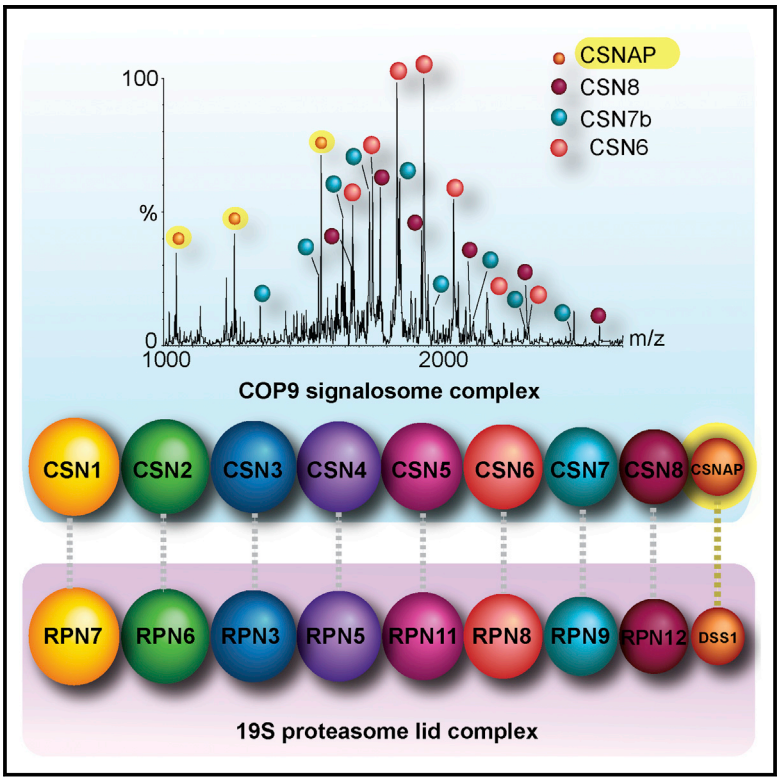


## Highlights

- CSNAP is the ninth subunit of the CSN complex
- CSNAP incorporation into the CSN is mediated through its C-terminal F/D-rich region
- Depletion of CSNAP leads to reduced cell proliferation
- CSNAP and the 19S proteasome lid subunit, DSS1, are most likely paralogs

## Authors

Shelly Rozen, Maria G. Füzesi-Levi, Gili Ben-Nissan, ..., Shifra Ben-Dor, Miriam Eisenstein, Michal Sharon

## Correspondence

michal.sharon@weizmann.ac.il

## In Brief

The highly conserved COP9 signalosome (CSN) complex is a key regulator of all cullin-RING-ubiquitin-ligases (CRLs), the largest family of E3 ubiquitin ligases. Rozen et al. report the discovery of an additional integral and stoichiometric subunit for this highly conserved complex.

Rozen et al., 2015, Cell Reports *13*, 585–598
October 20, 2015 ©2015 The Authors
http://dx.doi.org/10.1016/j.celrep.2015.09.021

Cell Reports
Article



# CSNAP Is a Stoichiometric Subunit of the COP9 Signalosome

Shelly Rozen,[1,5] Maria G. Füzesi-Levi,[1,5] Gili Ben-Nissan,[1,5] Limor Mizrachi,[1] Alexandra Gabashvili,[2] Yishai Levin,[2] Shifra Ben-Dor,[3] Miriam Eisenstein,[4] and Michal Sharon[1,*]
[1]Department of Biological Chemistry
[2]The Nancy and Stephen Grand Israel National Center for Personalized Medicine
[3]Biological Services Unit
[4]Chemical Research Support
Weizmann Institute of Science, Rehovot 7610001, Israel
[5]Co-first author
*Correspondence: michal.sharon@weizmann.ac.il
http://dx.doi.org/10.1016/j.celrep.2015.09.021


## SUMMARY

**The highly conserved COP9 signalosome (CSN) complex is a key regulator of all cullin-RING-ubiquitin ligases (CRLs), the largest family of E3 ubiquitin ligases. Until now, it was accepted that the CSN is composed of eight canonical components. Here, we report the discovery of an additional integral and stoichiometric subunit that had thus far evaded detection, and we named it CSNAP (CSN acidic protein). We show that CSNAP binds CSN3, CSN5, and CSN6, and its incorporation into the CSN complex is mediated through the C-terminal region involving conserved aromatic residues. Moreover, depletion of this small protein leads to reduced proliferation and a flattened and enlarged morphology. Finally, on the basis of sequence and structural properties shared by both CSNAP and DSS1, a component of the related 19S lid proteasome complex, we propose that CSNAP, the ninth CSN subunit, is the missing paralogous subunit of DSS1.**

## INTRODUCTION

The COP9 signalosome (CSN) complex is an evolutionarily conserved protein complex that exists in all eukaryotes (for reviews, see Schwechheimer, 2004; Wei et al., 2008). It contains eight canonical subunits that are termed CSN1 through CSN8, according to the descending order of molecular weights. The complex was originally identified as an essential factor that regulates light-induced development in *Arabidopsis thaliana* (Chamovitz et al., 1996; Wei et al., 1994); since then, it has been shown to play a critical role in diverse cellular processes including early development, DNA repair, cytokine signaling, regulation of nuclear transport, cell-cycle progression, angiogenesis, and antigen-induced responses (Schwechheimer, 2004; Wei et al., 2008). The involvement of the CSN in multiple cellular pathways is tied to its biochemical function as a regulator of the ubiquitin proteasome degradation pathway (Adler et al., 2006). Specifically, CSN coordinates the activity of cullin-RING ligases (CRLs) (Adler et al., 2006; Deshaies and Joazeiro, 2009).

The CRLs are a family of ubiquitin E3 enzymes that conjugate ubiquitin onto target proteins, thereby exerting a huge impact on cellular regulation (Deshaies and Joazeiro, 2009). Ubiquitination frequently leads to degradation of the target protein; indeed, ~20% of proteasome-dependent degradation is mediated by CRL ubiquitination (Soucy et al., 2009). Yet, in some cases, CRL-dependent ubiquitination acts as a switch to activate, repress, or relocalize target proteins. The CSN deactivates CRL function in two ways: (1) by deconjugation of the ubiquitin-like protein Nedd8 from the cullin subunit (deneddylation), an enzymatic process carried out by CSN5 (Cope et al., 2002); or (2) by physically binding to deneddylated CRLs, precluding interactions with E2 enzymes and ubiquitination substrates (Emberley et al., 2012; Enchev et al., 2012; Fischer et al., 2011). In mammals, the CRL family comprises eight cullin members (Cul1–Cul7 and PARC) and hundreds of substrate receptor modules that enable specific ubiquitination of multiple proteins involved in diverse cellular processes (Lydeard et al., 2013). Thus, vigorous control of CRLs by the CSN is critical for an organism's normal development and survival. It is therefore not surprising that impairment of CSN function is linked with multiple cancers (reviewed in Lee et al., 2011; Richardson and Zundel, 2005; Zhang et al., 2013).

The recently determined crystal structure of the recombinant CSN (Lingaraju et al., 2014) exposed the dynamic and fairly extended conformation of this complex. In particular, its architecture is governed by two organizational centers (Lingaraju et al., 2014): an open horseshoe-shaped structure formed by the "winged helix" subdomains of the six PCI subunits (proteasome, COP9, and initiation factor 3) (Hofmann and Bucher, 1998), CSN1–CSN4, CSN7, and CSN8, and an elaborate bundle comprising the carboxy-terminal ends of each subunit. Sitting atop this platform is the heterodimer formed by the MPN (Mpr1p and Pad1p N terminal) (Aravind and Ponting, 1998; Glickman et al., 1998; Hofmann and Bucher, 1998) subunits, CSN5 and CSN6. Binding of neddylated CRLs to CSN triggers substantial remodeling of the complex, activating the isopeptidase activity of CSN5. Given that the CSN is a key regulator of all CRLs, a high degree of flexibility is essential to facilitates its binding to

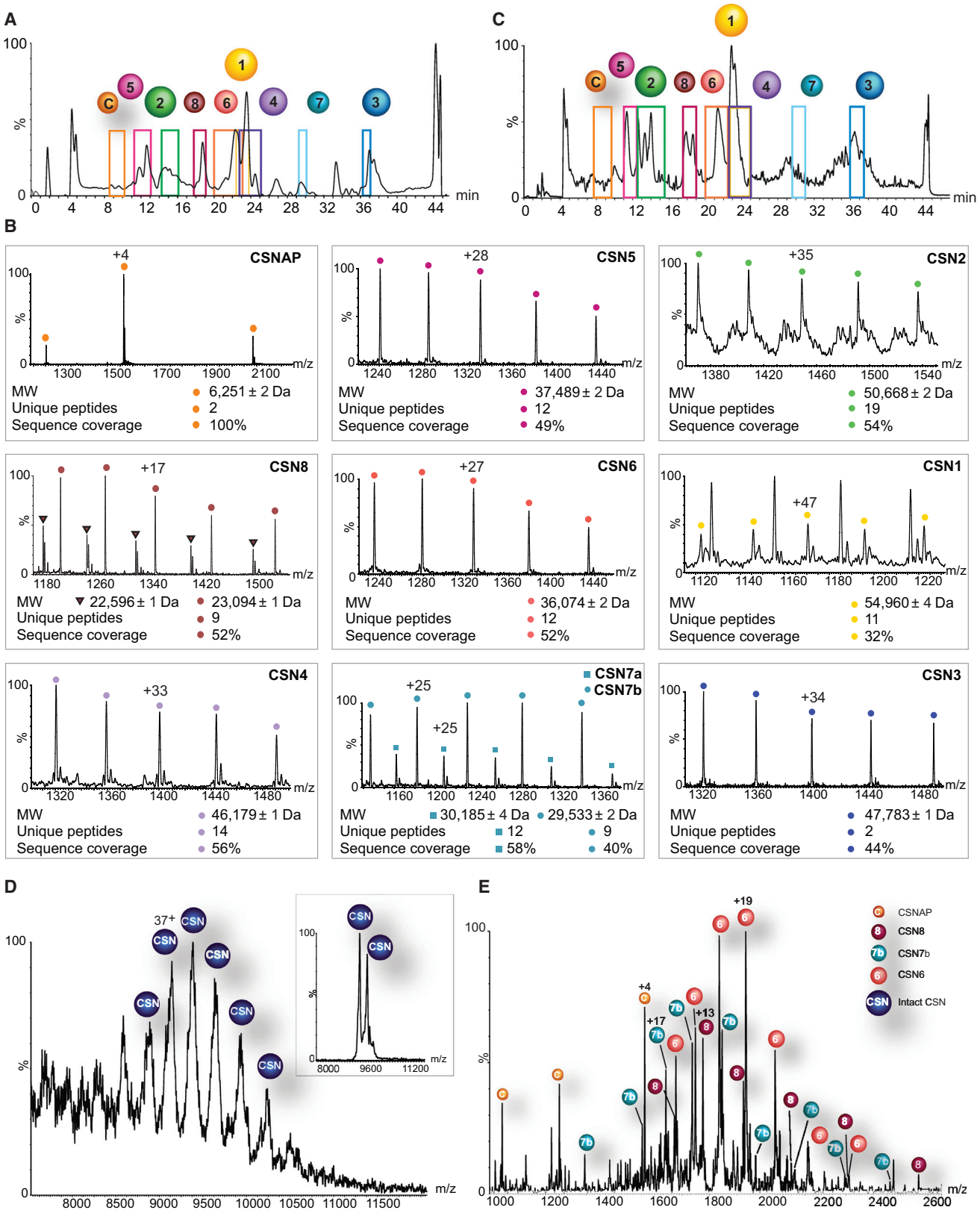


*(legend on next page)*

this structurally diverse family of more than 200 distinct complexes, including higher-order structures (Errington et al., 2012; Zhuang et al., 2009).

Notably, the CSN complex shares sequence similarities with two multi-subunit protein complexes: the lid component of the 19S proteasome and the eukaryotic translation initiation factor 3 (eIF3) (Glickman et al., 1998; Scheel and Hofmann, 2005; Seeger et al., 1998). While the eIF3 complex is more distinct and contains a larger number of subunits, the lid and the CSN exhibit a remarkable one-to-one correspondence between their two MPN and six PCI subunits. Beside this sequence homology, recent studies revealed that the two complexes also display similar architectures (da Fonseca et al., 2012; Enchev et al., 2012; Lander et al., 2012; Lasker et al., 2012; Lingaraju et al., 2014; Rockel et al., 2014). However, the 19S lid complex contains an additional small, non-PCI or MPN subunit, known as DSS1 (Sem1 in yeast), that has not yet been identified in the CSN assembly (Sone et al., 2004).

Here, we provide several lines of evidence indicating that a small, intrinsically disordered protein, which we named CSNAP (CSN acidic protein; previously named MYEOV2), is an integral subunit of the CSN complex. Our findings support results indicating that CSNAP is pulled down together with CSN subunits (Dunham et al., 2011; Ebina et al., 2013; Sowa et al., 2009). Moreover, we demonstrate that CSNAP, which is present at unit stoichiometry, tethers together the two distinct structural elements of the complex by mutually binding the MPN subunits, CSN5 and CSN6, and the PCI subunit CSN3. Furthermore, the C-terminal end of CSNAP, which is enriched with phenylalanine and aspartic acid residues, is crucial for its integration into the CSN. The lack of CSNAP yields a cellular phenotype characterized by reduced cell proliferation and a flattened and enlarged morphology. Finally, we suggest that CSNAP is the missing homologous subunit of DSS1, the only 19S lid subunit missing a counterpart in the CSN.

## RESULTS

### The CSN Complex Associates with CSNAP

Once the endogenous CSN complex was isolated from human erythrocytes, we examined its composition using a liquid chromatography mass spectrometry (LC-MS)-based approach that we recently developed (Rozen et al., 2013). This method, which couples bottom-up and top-down MS analysis, enables characterizing the protein complexes' subunit composition. Initially, the constituent subunits are separated on a column under denaturing conditions. Following subunit elution from the column, the flow is split into two fractions. One fraction is directed straight into the mass spectrometer for intact protein mass measurements, while the rest of the flow is fractionated into a 96-well plate, for subsequent peptide sequencing and subunit identification. The heterogeneity of subunit composition is then determined by correlating the subunit mass with its sequence identity.

By applying the LC-MS approach, all eight subunits of the CSN complex could be separated, including the two isoforms of CSN7 (Figure 1; Table S1). Data analysis demonstrated that all CSN subunits except for CSN1, CSN2, and CSN8 lack the first methionine (Met) residue and carry an N-terminal acetylation. In addition, the molecular mass of CSN2 suggests that the protein is a product of an alternative translation site at Met9. Similarly, two alternatively translated forms of CSN8 were identified: the mass of the heavier CSN8 variant corresponds to the removal of the first methionine, and the lighter form is a product of an alternative translation initiation site at Met6. The relative intensity of the two forms indicated that only ~30% of the CSN8 integrated within the CSN complex corresponds to the shorter form of the subunit, while the majority of CSN8 corresponds to the full-length protein.

Beyond the inherent diversity of CSN subunits, we noted the repetitive co-elution (retention time: 8 min) of an additional component, along with CSN subunits (Figures 1A and 1B). According to online MS measurements, we determined that this is a small protein, with a molecular weight of 6.2 kDa. Proteomic analysis identified the protein as myeloma overexpressed gene 2 (MYEOV2), which from now on we refer to as CSNAP, for CSN acidic protein. As will become apparent, CSNAP is the ninth subunit of the CSN complex. Though this subunit could have been named CSN9, this already designates the CSN7-like subunit of *Saccharomyces cerevisiae* (Maytal-Kivity et al., 2003).

To determine whether CSNAP specifically interacts with the CSN complex, rather than being a contaminate protein, we purified the complex from a different source: HEK293T cells stably expressing a FLAG-tagged CSN2 subunit. Because entirely different purification strategies were applied to isolate the CSN complex in each system (multi-column biochemical purification for erythrocytes and a single-step FLAG protocol for HEK293T cells) and there are great differences between these two cell types, it is unlikely that a similar contaminant protein would co-elute with the CSN in both systems. The subunit elution profile of the CSN complex isolated from HEK293T cells was very

**Figure 1. CSNAP Physically Associates with the CSN Complex**

(A–C) The endogenous CSN complex isolated from human erythrocytes (A and B) and HEK293 cells (C) was separated into its component subunits, using a monolithic column under denaturing conditions. A colored frame highlights the retention time of each eluted protein (A and C). CSNAP (labeled as C) was persistently detected alongside the eluted CSN subunits, implying its association with the CSN complex.

(B) The resulting electrospray ionization quadrupole time-of-flight mass spectra are shown. These spectra made it possible to determine the mass of the eluted protein and its associated variants; proteomics analysis was performed for sequence identification. CSNAP repeatedly co-eluted with the CSN subunits, suggesting that it associates with the complex. Indicated masses are an average of biological and technical measurements. Subunit variants are differentiated by labeling with circles and squares.

(D) Nano-electrospray mass spectrum recorded under native conditions of the human CSN complex isolated from HEK293T cells. The intact CSN complex is observed between 8,500 and 10,500 m/z. The $36^+$ and $35^+$ charge states (inset) were selected for MS/MS analysis.

(E) MS/MS spectrum showing the individual subunits stripped from the CSN complex. In addition to the dissociation of CSN6, CSN7b, and CSN8, we could also assign peaks corresponding in mass to CSNAP, indicating that it interacts with the CSN complex. The different species are denoted with labeled circles.

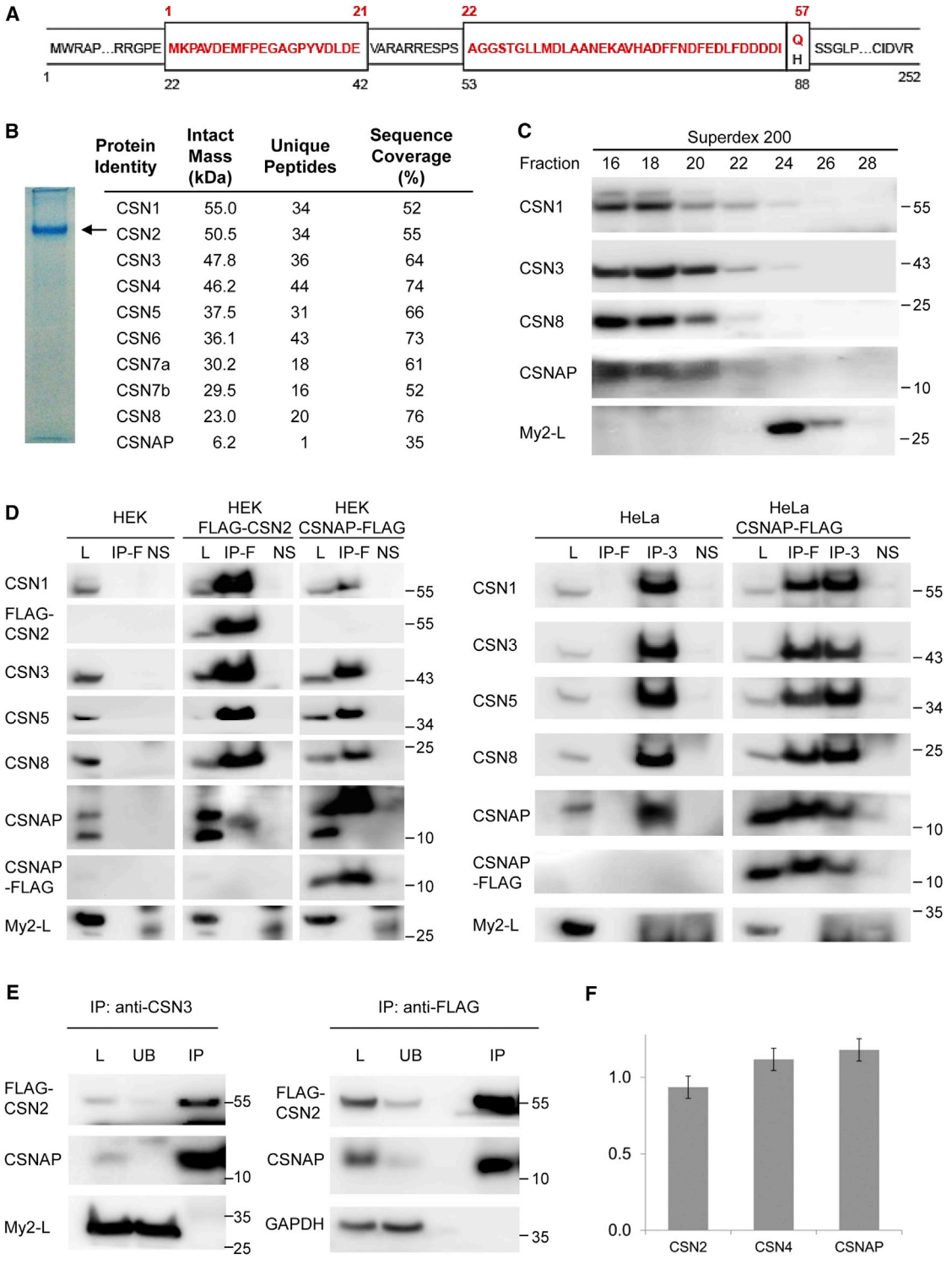


**Figure 2. The Short Isoform of the MYEOV2 Gene, CSNAP, Interacts with the CSN Complex**

(A) Schematic representation of the two alternatively spliced products of the MYEOV2 gene. Amino acid residues colored in red represent the CSNAP sequence (57 amino acids). The long MYEOV2 protein (252 amino acids, My2-L) contains the entire sequence of the short transcript except for glutamine 57, as well as additional sequence stretches in internal and end regions (shown in black).

(B) Native PAGE separation (6%) of the purified CSN complex. The position of the complex is denoted by an arrow; the absence of additional bands in the gel indicates the high integrity of the complex. Proteins extracted from the labeled band were subjected to proteomic LC-MS/MS analysis. Identified proteins with sequence coverage ≥30% are listed.

*(legend continued on next page)*

similar to that obtained for the CSN isolated from erythrocytes (Figure 1C).

Apart from the CSN subunits, we identified additional proteins common to both erythrocytes and HEK293 cells that were co-purified with the CSN (Table S2). These include expected members of the ubiquitin-proteasome system, the proteasome inhibitor PI31, SKP1, a member of the SCF (Skp1-cullin-F-box protein) complex, as well as chaperones and cytoskeleton-related proteins. Included among these proteins was also CSNAP (Figure 1C), suggesting that it is not a contaminant protein but rather a specific binding partner of the CSN complex.

## CSNAP Physically Binds the CSN Complex

To determine whether CSNAP physically interacts with the CSN complex, we applied the native MS approach under conditions that maintain non-covalent interactions between protein subunits (Sharon, 2013). In this experiment, the intact CSN complex appeared as a charge state series at ~9,500 m/z (Figure 1D). However, due to the diversity of CSN subunits (Table S1) and CSNAP's small size, it was impossible to determine unambiguously whether it binds to the CSN. Therefore, tandem MS (MS/MS) experiments were performed, in which a single peak corresponding to CSN ions was isolated. The ions were then subjected to collisional activation, and the individual subunits stripped from the complex were identified (Sharon, 2013). This process yielded not only the dissociation of canonical CSN subunits as CSN8, CSN7b and CSN6 but also the ejection of CSNAP (Figure 1E). By extrapolation, we can conclude that prior to the MS/MS analysis, CSNAP was bound to the CSN complex.

## The Short Isoform of CSNAP Is a Component of the CSN Complex

The MYEOV2 gene comprises two alternatively spliced isoforms (Figure 2A). The first encodes a protein containing 57 amino acids (molecular weight: 6.2 kDa), which we termed CSNAP. The second transcript generates a 252-amino-acid-long protein, with a calculated molecular weight of 27.7 kDa, known as MYEOV2-L. Even though the sequence of the shorter variant, CSNAP, is embedded within MYEOV2-L, we can unambiguously distinguish between the two proteins via proteomic analysis. This is because MYEOV2-L contains a short sequential insert between residues 43 and 52, and CSNAP includes a unique C-terminal glutamine residue (Gln57). Considering that our LC-MS analysis (Figure 1) involved both molecular weight measurements and proteomic analysis, we could clearly demonstrate that CSNAP is the variant associated with the CSN. Nevertheless, we wished to determine whether MYEOV2-L could also interact with the complex.

We began by separating the endogenous CSN complex on a 6% native PAGE (Figure 2B). Only a single band was detected in the gel, indicating not only the high purity of the sample but also the stability of the complex. We then extracted the proteins from the band and performed a proteomic LC-MS/MS analysis using a 30% sequence identity coverage cutoff. Together with the eight canonical CSN subunits, CSNAP, but not MYEOV2-L, was also identified (Figure 2B, right panel), suggesting that unlike CSNAP, MYEOV2-L is not a component of the CSN complex.

To further strengthen our results, we generated a polyclonal antibody against a synthetic peptide containing the entire CSNAP sequence, which recognized both the CSNAP and MYEOV2-L isoforms. We then performed a gel filtration analysis of HEK293 cell extract to monitor whether these proteins co-elute with the CSN complex. Western blot analysis indicated that CSNAP displays an elution profile similar to those of CSN1, CSN3, and CSN8, while MYEOV2-L elutes at lower-molecular-weight fractions (Figure 2C), supporting our premise that MYEOV2-L is not part of the CSN complex.

Next, reciprocal co-immunoprecipitation experiments were performed using both HeLa and HEK293 cell extracts (Figure 2D). The results obtained for the two cell lines were virtually the same: When cells transiently expressing CSNAP-myc-FLAG were co-immunoprecipitated using an anti-FLAG resin, CSN1, CSN3, CSN5, and CSN8 were pulled down. When anti-CSN3 was used for pull-down in HeLa cells, the antibody directed toward CSNAP gave rise to two bands: an intense band at CSNAP's molecular weight and a second, faint band corresponding in size to MYEOV2-L. Notably, the intensity of the MYEOV2-L band was similar to the nonspecific signal that appeared when non-conjugated beads were used as a negative control, suggesting that this faint band is a product of a nonspecific interaction. When we used HEK293T cells stably expressing FLAG-CSN2 and an anti-FLAG resin, CSNAP, but not MYEOV2-L, was pulled down. Similar results were also obtained when reciprocal co-immunoprecipitation experiments were performed

(C) HEK293T FLAG-CSN2 cell extract was subjected to Superdex 200 gel-filtration chromatography. Fractions were collected and analyzed by SDS-PAGE and immunoblotting. CSNAP co-fractionated with the CSN complex, unlike MYEOV2-L, that eluted in lower-molecular-weight fractions. In all western blots, molecular weights are indicated in kDa units. All experiments were repeated at least three times.

(D) Whole-cell lysates (L) from HEK293T (HEK) cells stably expressing FLAG-CSN2, or HEK293 cells transiently expressing CSNAP-FLAG (left panel), as well as lysates from HeLa cells transiently expressing CSNAP-FLAG (right panel), were subjected to immunoprecipitation (IP) using FLAG affinity gel (IP-F) or anti-CSN3 antibody (IP-3). Pull-downs were analyzed by western blots using antibodies against CSN subunits, CSNAP, and FLAG. The results show that CSNAP, but not the long version of MYEOV2, co-immunoprecipitates with the CSN complex. As controls, wild-type HEK293 and HeLa lysates were used. To rule out non-specific interactions, lysates were also incubated with Protein G Sepharose, without the addition of the primary antibodies (NS).

(E) CSN was co-immunoprecipitated from HEK293 stably expressing FLAG-CSN2, using an anti-CSN3 antibody or anti-FLAG resin. The whole-cell lysates (L) bound (IP) and unbound (UB) fractions were analyzed by western blots using antibodies against CSNAP and FLAG. GAPDH and My2-L were used as negative controls. The depletion of CSN2 and CSNAP from the unbound fraction suggests not only that the majority of CSN complexes are bound to CSNAP but also that this small protein is not part of another protein complex.

(F) CSN was subjected to targeted proteomic analysis by selective reaction monitoring (SRM) mass spectrometry and stable, isotopically labeled peptide standards. Absolute quantification was done by referencing the native peptide intensities to the heavy labeled standards and then normalizing against a representative peptide. Results indicate that CSN subunits and CSNAP are present in equimolar amounts. Data shown are the result of three biological replicates, with two technical replicates each. Error bars indicate the SDs of all six measurements.

using A31N-ts20 BALB/c mouse embryo fibroblast cells (Figure S1). Moreover, pull-down assays using anti-FLAG resin or an anti-CSN3 antibody depleted both CSNAP and FLAG-CSN2 from the unbound fraction, unlike MYEOV2-L or GAPDH, respectively (Figure 2E). This result suggests that cellular CSNAP is present in the majority of CSN complexes. Altogether, the data imply that only CSNAP, and not MYEOV2-L, is a bona fide member of the CSN complex.

## CSNAP Is a Stoichiometric Subunit of the CSN Complex

To determine whether CSNAP is a stoichiometric component of the CSN, we subjected the anti-CSN3 immunoprecipitated complex to targeted proteomic analysis by selective reaction monitoring (SRM) MS for absolute quantification (based on the AQUA approach) (Ménétret et al., 2007). Custom stable-isotope-labeled peptides of CSN2, CSN4, and CSNAP were synthesized and quantified by amino acid analysis. Those were spiked into the complex samples, enabling absolute quantification of the CSN and CSNAP subunits by converting light/heavy peak area ratios into absolute protein amounts. Values were then normalized against a representative peptide (Figure 2F). We found that the measured stoichiometry of CSN2, CSN4, and CSNAP was ~1:1:1, indicating that CSNAP, like the other CSN subunits, is present in equimolar amounts.

## The C-Terminal F/D-Rich Region of CSNAP Mediates Its Association with CSN, with Phe44 and Phe51 Playing Direct Roles in the Interaction

To clarify which domain within CSNAP mediates its interaction with the CSN complex, we transiently expressed several versions of CSNAP, including deletion mutants of either the N- or C-terminal regions, fused to the fluorescent protein Cerulean (Cer) in HEK293 cells (Figure 3A). Initially we examined the cellular localization of CSNAP. Full-length CSNAP constructs were seen throughout the cytoplasm and nucleus but were excluded from nucleoli (Figure S2), as previously observed for other CSN subunits (Füzesi-Levi et al., 2014). We then performed reciprocal co-immunoprecipitation analyses, using antibodies against CSN3 and GFP (Figure 3B). The results indicated that fusing Cer to either terminus of CSNAP did not hinder its ability to interact with CSN. Likewise, deletion of the N-terminal region of CSNAP did not affect the CSNAP/CSN association. However, CSNAP was unable to bind CSN in the absence of the C-terminal fragment, suggesting that this region is essential for interaction with the complex.

Analysis of the amino acid sequence of CSNAP indicates that it is enriched with charged and polar amino acids, characteristic of intrinsically disordered proteins (Dyson and Wright, 2005). Such proteins, however, tend to adopt distinct structures in their bound state. When we examined CSNAP's C-terminal sequence, the region critical for its incorporation into the CSN, we noticed not only that it is rich in phenylalanine and aspartic residues (F/D-rich domain) but also that the two types of residues are alternately spaced three and four residues apart. This observation suggests that this C-terminal region might adopt a binding configuration of an amphipathic $\alpha$-helix containing both aromatic and negatively charged sides (Figure 3C). It is therefore reasonable to assume that the aromatic face is buried within the complex forming the CSNAP/CSN interface.

To test this hypothesis, single and double mutants were introduced into ΔN-CSNAP-Cer at positions 44 and 51 (F44A, F51A, F44A-F51A). The mutant proteins were transiently expressed in HEK293 cells, and subjected to reciprocal co-immunoprecipitation with antibodies against CSN3 and GFP (Figure 3D). Though the F44A mutation did not interfere with the CSNAP/CSN interaction, and binding of the F51A CSNAP mutational variant to CSN was noticeably reduced, it was the F44A-F51A double mutant that displayed the most striking phenotype, completely abolishing the ability of CSNAP to interact with the CSN. Therefore, within the F/D-rich C-terminal region of CSNAP, F44 and F51 are necessary mediators of its interaction with the CSN.

## Cellular Analyses Indicate that CSNAP Is an Integral Subunit of the CSN Complex

We recently demonstrated that following induction of UV damage, the CSN complex is transiently recruited to the nucleoplasmic and chromatin fractions (Füzesi-Levi et al., 2014). We therefore wished to explore whether CSNAP acts as an integral CSN component and displays a similar relocalization pattern. To this end, HeLa cells were exposed to UV irradiation, and cells were then fractionated (Figure 4A). Our findings indicated that the level of cytosolic CSNAP did not significantly change in response to UV irradiation, though a clear increase in CSNAP intensity was observed in the nucleoplasmic and chromatin-associated fractions immediately after UV irradiation, as observed for CSN subunits. However, no change in the intensity levels of MYEOV2-L was detected. This finding confirms the analogous cellular response of CSNAP and the CSN complex.

To study the diffusion kinetics of CSNAP in live cells, we performed fluorescence recovery after photobleaching (FRAP) measurements in both the cytosol and nuclear compartments of HEK293 cells stably expressing different fluorescently tagged CSNAP constructs (Luijsterburg et al., 2007). Previously, we had demonstrated that the recovery curves of CSN2, CSN3, CSN6, and CSN7 subunits are very similar, indicating that they commonly reside within the holo-CSN complex (Füzesi-Levi et al., 2014). Thus, if CSNAP is an integral subunit of the complex, it is expected to display comparable mobility. For comparison, we conducted similar measurements on cells stably expressing free Cer and Cer-CSN3, representing the dynamics of a fully mobile, monomeric protein (Dross et al., 2009) and the CSN complex, respectively. As an additional control, we used cells stably expressing fluorescently tagged DDB2, a nuclear DNA-binding protein previously shown to interact with the CSN, though not an integral subunit of the complex (Groisman et al., 2003; Olma et al., 2009).

Examination of the resulting data indicated that Cer-CSNAP and Cer-CSN3 recovery curves were remarkably similar, displaying significantly slower mobility compared to that of free Cer, and suggesting that Cer-CSNAP is part of the CSN complex (Figures 4B and S3). In contrast, the mobility kinetics of the CSNAP construct lacking the C-terminal F/D region were comparable to that of free Cer, further demonstrating that this region is critical to CSNAP incorporation into the CSN. The absence of the N-terminal region did not affect the recovery rate, which was similar to that of Cer-CSNAP and Cer-CSN3, suggesting that the

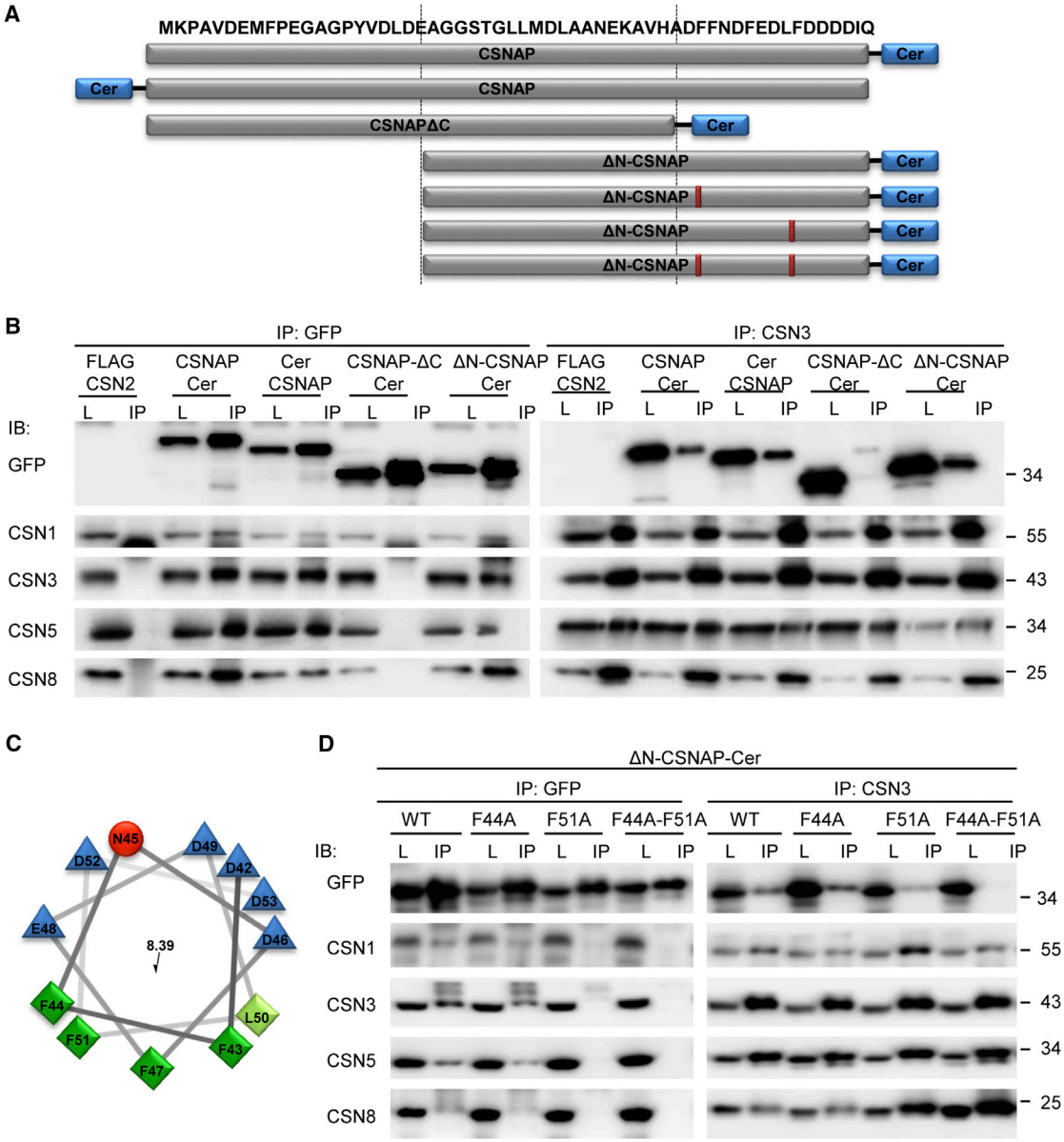


**Figure 3. The F/D-Rich C-Terminal Domain of CSNAP, Specifically Phe44 and Phe51, Is Involved in Its Interaction with the CSN Complex**

(A) Schematic representation of the different CSNAP constructs used in this experiment.

(B) Cellular proteins extracted from the different fluorescently tagged HEK293 cell lines were immunoprecipitated, using anti-GFP and anti-CSN3 antibodies. As control, lysate from HEK293 cells stably expressing FLAG-CSN2 was used. Lysates (L) were run side by side with their corresponding immunoprecipitated proteins (IP) and visualized using various antibodies, as indicated (IB). Results show that CSNAP-ΔC-Cer did not interact with the CSN, indicating that the C-terminal domain is responsible for its interaction with the complex.

(C) Helical wheel representation of the CSNAP C-terminal region. Hydrophilic and hydrophobic residues are colored blue and green, respectively. Distribution of the residues on either side of the helix suggests amphipathic properties for this structure.

(D) Lysates (L) from HEK293 cells expressing ΔN-CSNAP-Cer (WT) and its mutational variants, consisting of single (F44A and F51A) and double (F44A-F51A) amino acid substitutions, were immunoprecipitated by either anti-GFP or anti-CSN3 (IP). Pull-downs were analyzed by western blot, using antibodies against GFP and CSN subunits. Findings show that while Phe44 displacement yielded results similar to those of the WT construct, the F51A mutant extensively weakened the interaction of ΔN-CSNAP with the CSN. The most pronounced effect was observed for the F44A-F51A double mutant, which entirely abolished the ΔN-CSNAP/CSN interaction.

F/D region alone is sufficient for CSNAP/CSN assembly. In the nucleus, DDB2 exhibited a clearly slower recovery compared to that of Cer-CSN3 and Cer-CSNAP, reflecting some degree of transient immobilization. Taken together, the similar mobility kinetics of CSNAP and CSN3 strongly suggest that CSNAP is an integral component of the holo-CSN complex.

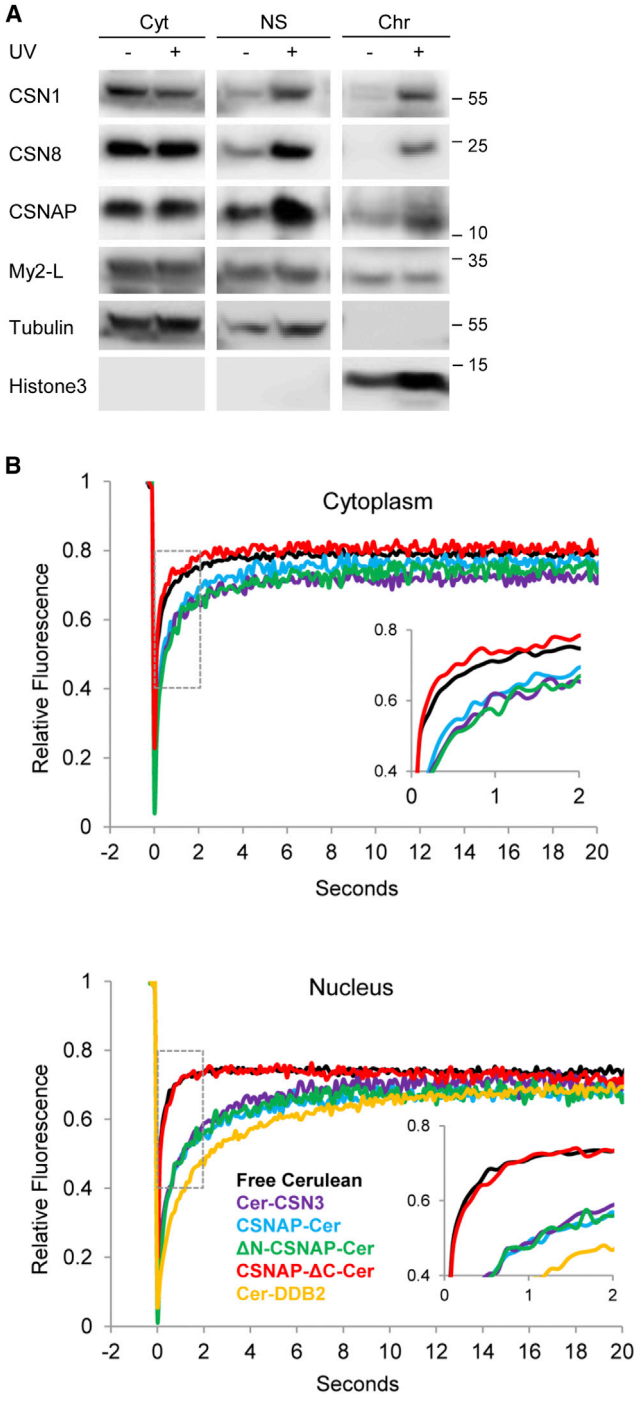


**Figure 4. Live Cellular Analyses Indicate that CSNAP Is an Integral CSN Subunit**

(A) HeLa cells were fractionated into cytoplasmic, nuclear soluble, and chromatin-associated fractions, with or without prior exposure to UV light. Fractions were separated on tricine-SDS gels, and blots were probed with anti-CSN1, CSN8 and CSNAP antibodies. As controls, anti-tubulin and anti-histone 3 antibodies were used. Like CSN subunits, CSNAP, but not MYEOV2-L (My2-L), is recruited to the nucleoplasmic and chromatin fractions following DNA damage induction.

(B) FRAP curves of full-length CSNAP-Cer, as well as its deletion mutants, ΔN-CSNAP-Cer and CSNAP-ΔC-Cer, were compared to those obtained for free Cer and fluorescently labeled CSN3 and DDB2. Each plot constitutes an average of at least 40 cells, normalized to pre-bleach intensity. To better display the mobility differences between the measured cell lines, the regions within the dashed squares were enlarged (insets).

## CSNAP Interacts with CSN3, CSN5, and CSN6

To determine which of the CSN subunits binds CSNAP, we performed chemical cross-linking reactions using $BS^3$, a homobifunctional amine-reactive compound that reacts predominantly with the primary amines in lysine side-chains, and the N termini of polypeptide chains (Kalkhof and Sinz, 2008). We then monitored the change in the protein's band pattern by running denaturing gel electrophoresis (SDS-PAGE) before and after cross-linking. Immunoblotting with anti-CSNAP and various anti-CSN antibodies revealed the appearance of similarly sized, higher-molecular-mass species for CSNAP and CSN3, CSN5, and CSN6 (Figure 5A). The CSNAP-CSN3, CSNAP-CSN5, and CSNAP-CSN6 bands were sensitive to the presence of a denaturing agent: when SDS was added and the sample was boiled prior to the cross-linking reaction, the cross-linked species were eliminated, implying the specificity of the interaction (Figure 5A). In contrast, cross-links with CSNAP were not identified for CSN1, CSN2, and CSN8.

Despite numerous attempts, we were unable to map the specific sites of association between CSNAP and CSN3, CSN5, and CSN6 using proteomic MS analysis. This is likely due to CSNAP's relatively small size and the few peptides it produces, reducing the odds of identifying explicit CSNAP cross-linked species within the complex mixture of CSN peptides. Nonetheless, when we examined the recently solved crystal structure of the recombinant CSN complex (Lingaraju et al., 2014), the only region in which CSN3, CSN5, and CSN6 are in proximity, and their surfaces not obscured by the other subunits, is near the C-terminal helices of CSN3 and CSN6, and the loop 284-295 of CSN5, which connects its two C-terminal helices (Figure 5B). Near this region, we noted a highly positive patch on the CSN3 surface that contains several exposed lysine residues capable of forming a cross-link with CSNAP. Lysine residues of CSN5 and CSN6, which could act as additional cross-link targets, are located near the CSN3 positive patch (Figure 5C). This patch, which corresponds to the PCI domain of CSN3, includes several hydrophobic pockets, which are preferred phenylalanine binding sites as determined by ANCHORSmap (Ben-Shimon and Eisenstein, 2010). From the crosslinking results, and the structural features of CSNAP and the CSN subunits, we suggest that the positive patch of CSN3 binds the CSNAP F/D-rich motif by forming ionic interactions with the negative charges and hydrophobic interactions with CSNAP Phe44, Phe51, and perhaps also Phe47. Other parts of CSNAP bind near the helical bundle region, thus tethering the MPN dimer of CSN5 and CSN6 to the PCI proteins, through CSN3.

## CSNAP and DSS1 Share Sequential and Structural Properties

At this point, we referred to the related 19S lid complex, which shares one-to-one subunit correspondence with the CSN,

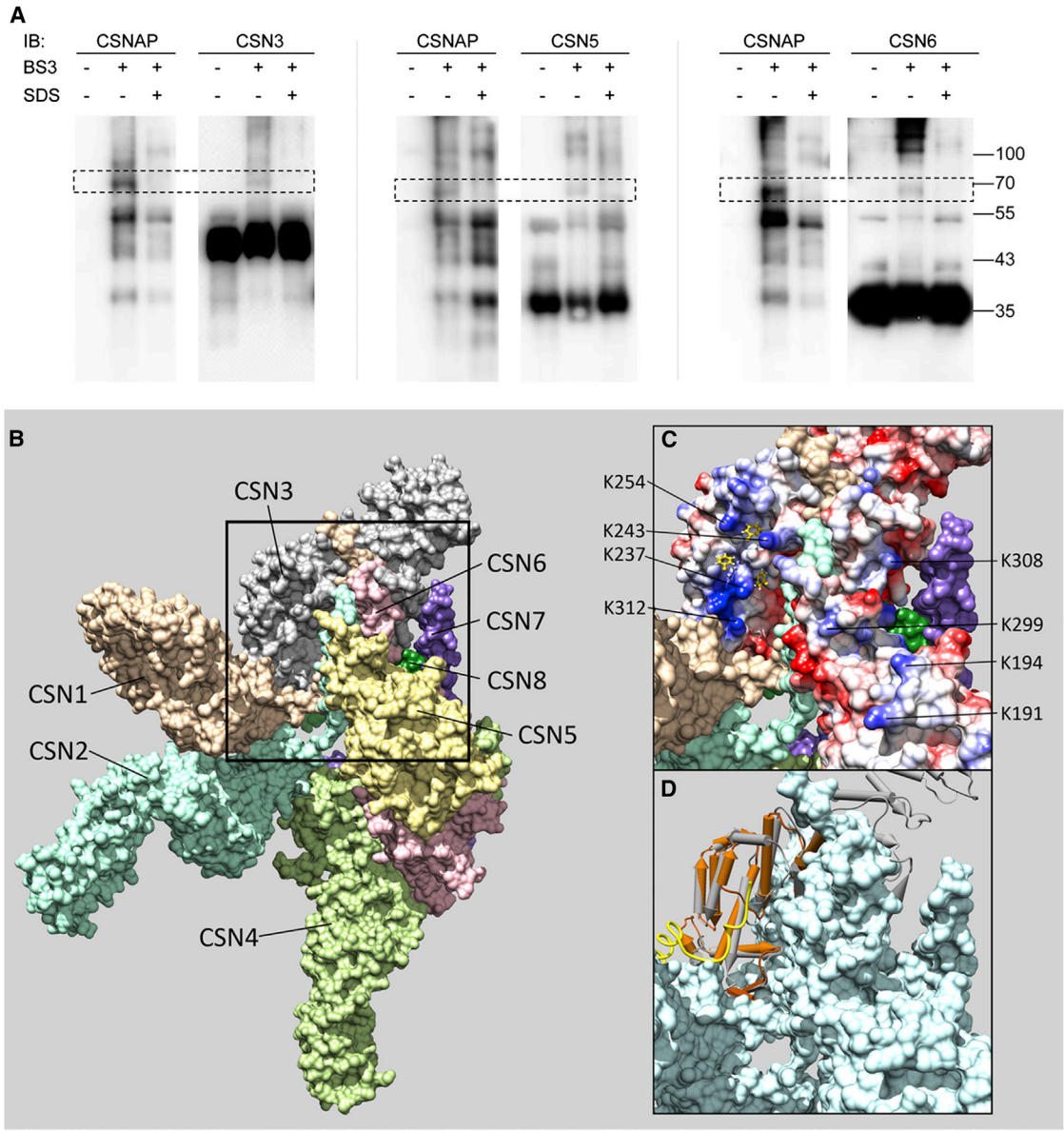


**Figure 5. CSNAP Interacts with CSN3, CSN5, and CSN6**

(A) FLAG-tagged CSN was purified from HEK293T cells and cross-linked with $BS^3$. As a control for specific CSNAP association, FLAG-CSN was denatured with 1% SDS and boiled for 5 min, prior to addition of the cross-linker. After quenching the reaction, the complex was precipitated with acetone, followed by western blot analysis with antibodies against CSNAP and CSN subunits. The data revealed that CSNAP forms a cross-link with CSN3, CSN5, and CSN6.

(B) An overall view of the CSN crystal structure, showing the surfaces of the eight subunits (Lingaraju et al., 2014). The black frame delineates the region where CSN3, CSN5, and CSN6 are found in close proximity. This region, enlarged in (C) and (D), includes the C-terminal helices of CSN3 and CSN6 and the loop 284–295 of CSN5, which connects its two C-terminal helices.

(C) The electrostatic potential on the surfaces of CSN3, CSN5, and CSN6: blue for positive, red for negative, and white for neutral. The highly positive patch of CSN3 is seen at the top left. Exposed lysine residues that may be involved in cross-linking are indicated: K237, K243, K254, and K312 of CSN3; K191, K194, and K299 of CSN5; and K306 of CSN6. The positive patch includes several hydrophobic pockets, which are preferred anchoring sites of Phe residues, as predicted by ANCHORSmap. Anchored Phe side chains with $\Delta G < -4$ kcal/mol are shown in yellow.

(D) Superposition of the PCI domain of PCID2 (brown) in the complex with DSS1 (Ellisdon et al., 2012), onto the PCI domain of CSN3 (gray). The F/D-rich region of DSS1 (golden coil) binds to the front face of PCID2, which corresponds to the positive patch of CSN3.

except for DSS1, which is missing a counterpart. We noticed, however, that CSNAP and DSS1 not only share sequential similarity (Figure S4A) but also belong to the same intrinsically unstructured protein family (Figure S4B). Thus, CSNAP could potentially be the subunit homologous to DSS1 and, as such, may occupy a similar position within the CSN architecture.

The molecular architecture of the 26S holocomplex was recently determined using cryo-electron microscopy single-particle analyses; however, the position of DSS1/Sem1 within the lid was not resolved due to its small size (Beck et al., 2012; Lander et al., 2012; Lasker et al., 2012). Nevertheless, cross-linking analysis and biochemical characterization indicated that DSS1/Sem1 forms a subcomplex with RPN3 and RPN7, enforcing their joint incorporation into the lid (Fukunaga et al., 2010; Sharon et al., 2006; Tomko and Hochstrasser, 2014). Comparative cryo-electron microscopy maps and cross-linking restraints position DSS1/Sem1 in the cleft between the PCI domains of Rpn7 and Rpn3, while its central part lies near the N-terminal region of Rpn3. This mode of binding, near the 19S lid helical bundle, fastens the lid together (Bohn et al., 2013; Kao et al., 2012; Tomko and Hochstrasser, 2014). Based on the cross-linking results, it seems that CSNAP occupies an analogous binding mode in which it tethers the MPN subunits CSN5 and CSN6 to the PCI CSN3 subunit at the helical bundle region. More evidence of this binding mode is provided by superpositioning the PCI subunit of PCID2 in the PCID2/DSS1 complex (Ellisdon et al., 2012) onto the PCI domain of CSN3, showing that the DSS1 binding surface of PCID2 corresponds to the CSN3-positive patch, proposed here to be the CSNAP binding surface (Figure 5D). Small differences in the actual binding modes support the observation that CSNAP and DSS1/Sem1 are intrinsically unstructured proteins; therefore, their interaction partners co-determine their structure, as previously shown for DSS1 (Ellisdon et al., 2012; Yang et al., 2002). Overall, it suggests that like DSS1/Sem1, CSNAP connects subunits within the complex.

### CSNAP-Depleted Cells Display a Distinct Phenotype

To test whether CSNAP confers functional significance, HAP-1 cell lines lacking CSNAP (ΔCSNAP cells) were generated using the CRISPR system. Initially, pull-down assays using an anti-CSN3 antibody confirmed that CSNAP is absent from the CSN complex in the ΔCSNAP cell line (Figure 6A). Next, cell extracts of wild-type and ΔCSNAP cells were passed through a column containing CSNAP-conjugated beads. After washing, beads were boiled in SDS-PAGE sample buffer, and the bound proteins analyzed by western blots. We found that only CSN from the ΔCSNAP cells was able to bind the CSNAP-column, whereas that from the wild-type cells did not bind (Figure 6B). This result not only validated the lack of CSNAP in the engineered cells, it also confirmed the stoichiometric CSN/CSNAP association in wild-type cells.

We then examined whether the enzymatic activity of the ΔCSNAP and wild-type CSN complexes differ. No significant difference in the deneddylation capacity was observed between wild-type and ΔCSNAP cells (Figure 6C). This observation is in accordance with a previous study that compared the rate of deneddylation of endogenous CSN prepared from HEK293 cells with that of recombinant CSN expressed in insect cells (Emberley et al., 2012). Although the recombinant CSN might contain the insect CSNAP protein, it is unlikely to be stoichiometric, due to its very high overexpression levels. Thus, CSNAP might not have a significant effect on the enzymatic activity of the CSN.

Next, we examined whether the lack of CSNAP gives rise to a detectable cellular phenotype. To this end, we performed cell proliferation assays and compared the growth potential of wild-type and ΔCSNAP HAP-1 cells. Our data (Figure 6D) show that there is a clear reduction in cell proliferation in the ΔCSNAP clone compared to the wild-type cells. Furthermore, microscopy analysis of both cell types demonstrated that ΔCSNAP cells display a flattened and enlarged cell phenotype compared to wild-type cells (Figures 6E–6G). These results indicate that the lack of CSNAP generates a distinct phenotype, indicating the functional significance of this small subunit. Nevertheless, further research is required in order to determine the specific mechanistic function of CSNAP.

## DISCUSSION

Here, we show that CSNAP, a 6.2-kDa protein, is a stoichiometric subunit of the CSN complex. The protein's second, longer isoform, MYEOV2-L (27.7 kDa), which contains the entire sequence of CSNAP except for the C-terminal amino acid, is not, however, part of the complex. Moreover, we demonstrate that the C-terminal F/D-rich region of CSNAP is necessary and sufficient for its incorporation into the CSN and, in particular, conserved Phe44 and Phe51 take part in this interaction. Our data also demonstrate that CSNAP binds to CSN3, CSN5, and CSN6, possibly linking the MPN and PCI substructures. Finally, we found that the absence of CSNAP had a marked effect on the cellular morphology and proliferation rate. Although this result implies biological relevance, further investigation is required to determine the specific functional role of CSNAP. It is tempting to suggest that it contributes to the complex stability or flexibility, enabling the CSN to associate and dissociate from the variable CRL complexes.

CSNAP was first identified as an overexpressed gene in ARH-77 cells (Tang et al., 2003), which were considered to be cultures of human myeloma cells, giving the protein its original name, MYEOV2 (myeloma-overexpressed gene 2). Notably, however, these cells were shown to be a false malignant hematopoietic cell line, essentially representing Epstein-Barr virus (EBV)-transformed B lymphoblastoid cells (Drexler et al., 1999), a fact that supports our suggestion to rename the protein. Still, this study stimulated us to examine whether overexpression of CSNAP in ARH-77 cells is coordinated with the other CSN subunits, as expected of constituents of the same protein complex (Eisen et al., 1998; Jansen et al., 2002). Interestingly, analysis of microarray data using the GeneVestigator database revealed not only that the expression levels of the entire CSN complex, including CSNAP, are highly comparable in ARH-77 and various other cell lines (Figure S5A) but also that similar expression coherence is obtained across different tissues and organs (Figure S5B). Likewise, when we examined the expression patterns in a range of cancers (e.g., colon, leukemia, and lung) reported to induce overexpression of CSN5 and/or CSN6 (Adler et al., 2008; Chen et al., 2014), the entire CSN complex, including CSNAP, displayed similar expression levels (Figure S5C). Together, these results indicate that all CSN-encoding genes, including CSNAP, show similar expression patterns, as expected from subunits of the same protein complex (Jansen et al., 2002).

The first documentation concerning the existence of CSNAP at the protein level came from a global proteomic analysis

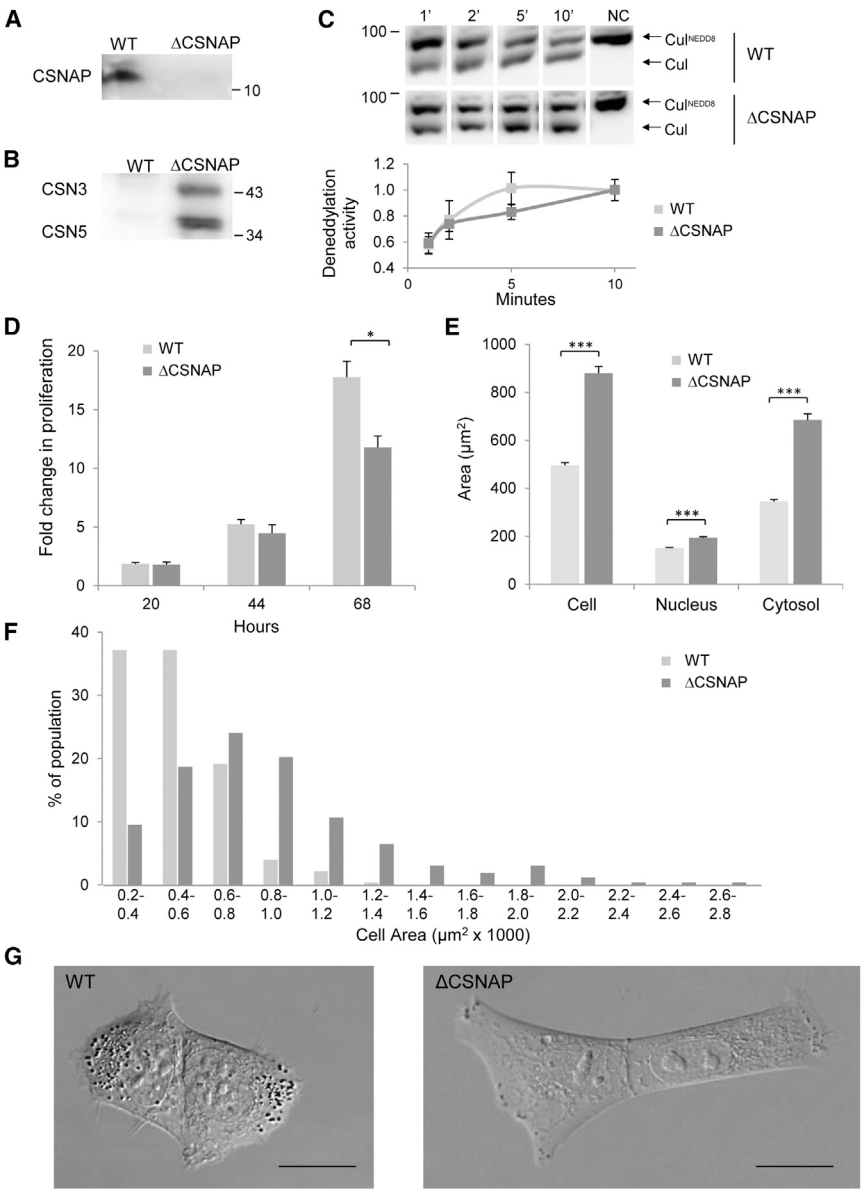


**Figure 6. CSNAP-Depleted Cells Display a Distinctive Phenotype**

(A) The CSN complex was FLAG-affinity purified from wild-type (WT) or from CSNAP knockout cells (ΔCSNAP), stably expressing FLAG-CSN1. CSNAP was detected by western blot using an anti-CSNAP antibody only in the complex isolated from WT, but not ΔCSNAP, cells.

(B) The WT CSN complex is saturated with endogenous CSNAP. Lysates from WT and ΔCSNAP cells stably expressing FLAG-CSN1 were passed through Aminolink beads coupled to a CSNAP-peptide. Only the CSN complex from the ΔCSNAP, but not from the WT lysate, could bind to the beads.

(C) WT and ΔCSNAP cells exhibit a similar rate of deneddylation. Deneddylation was monitored at different time points. A representative deneddylation assay (top panel) and a plot demonstrating the average activity of three independent experiments (bottom panel). As a negative control (NC), lysates were denatured (boiled) prior to the assay. Bars represent SE.

(D) ΔCSNAP cells exhibit lower proliferation rates, as measured using the resazurin proliferation assay. Plot represents the average proliferation rate of three independent experiments. Measurements were subjected to t test analysis; $^{*}p < 0.05$.

(E) ΔCSNAP cells are flatter and larger than WT cells. Cells plated at a low density were imaged using a confocal microscope. Partially dispersed cells displaying distinct cellular borders were used to measure the cellular area of WT (n = 277) and ΔCSNAP cells (n = 263). Bars represent SE. Measurements were subjected to t test analysis; $^{***}p < 10^{-15}$.

(F) Size distribution of WT and ΔCSNAP cell areas, represented as percent of the total population.

(G) A representative confocal image of WT and ΔCSNAP cells. Bar represents 20 μm.

aimed at identifying deubiquitinating enzyme-associated proteins (Sowa et al., 2009). The study indicated that CSNAP is pulled down, together with CSN6. Similarly, a methodological study focused on the effectiveness of multidimensional separation techniques for MS analysis indicated that MYEOV2 is repeatedly identified in FLAG-CSN5 purifications (Dunham et al., 2011). A later study, focusing on the subnuclear localization of the ribosomal L11 protein, indicated that overexpression of a FLAG-tagged construct containing the N-terminal region of MYEOV2-L, comprising the F/D-rich motif, is co-immunoprecipitated with CSN5, Cul1, and Cul3 (Ebina et al., 2013). In contrast, a construct containing the long, MYEOV2-L C-terminal tail could not interact with the CSN complex. Moreover, a genetic screen searching for *A. thaliana* mutants that display resistance to the auxin inhibitor p-chlorophenoxyisobutyric acid identified the small acidic protein 1 (SMAP1) (Rahman et al., 2006), the plant ortholog of CSNAP. A subsequent study indicated that SMAP1 physically binds the CSN complex via the F/D-rich region (Nakasone et al., 2012). Taken together, these results support our view that CSNAP is an integral component of the CSN complex.

The CSN complex is conserved throughout eukaryote evolution, from fungi to humans (Schwechheimer, 2004; Wei et al., 2008). Therefore, it would be expected that as a CSN component, CSNAP would be similarly conserved. To examine this possibility, we performed bioinformatics searches, the results of which indicated that CSNAP is highly conserved in all chordates and also displays a high degree of similarity in lower eukaryotes (Figure S6). In plants, conservation is mainly maintained in the C-terminal F/D-rich region, the domain essential for CSN integration. We could not, however, identify a yeast ortholog of CSNAP, perhaps because the protein diverged to such an extent that it is difficult to identify it by homology database searches;

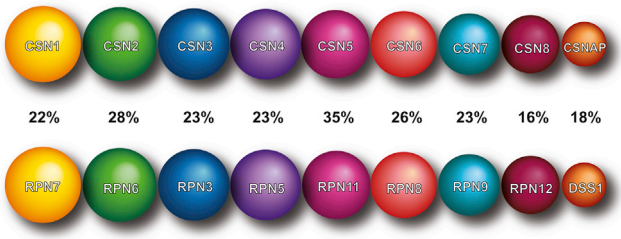


**Figure 7. DSS1 and CSNAP Are Intrinsically Disordered Proteins that Share Sequential and Functional Homology**

Schematic illustration of the one-to-one sequence homology between the CSN and 19S proteasome lid complexes. CSNAP may represent the missing homologous partner of DSS1. The percentage of sequence identity between the subunits is labeled for each pair.

rather, experimental approaches are required. More conservational support for the CSN/CSNAP link comes from the fact that CSN7b, CSN8, and CSNAP are all located in the same chromosomal region (2q37) and that they are found together in syntenic regions in all mammalian species (e.g., mouse, rat, horse, and pig) whose DNA sequences are available so far. In marsupials, there is no CSN7b gene; however, CSN8 and CSNAP are co-localized on the same chromosome. The shared synteny in mammals may reflect selection due to a functional relationship (Moreno-Hagelsieb et al., 2001), strengthening the link between CSNAP and the CSN.

Unlike CSNAP, there is very little transcriptional evidence that MYEOV2-L is expressed in humans; thus far, no such evidence has been found in other species at all (Figure S7). The lack of conservation in all non-primates makes it highly unlikely that it exists in those species. Even in primates, where the exon sequences are mostly present, the splice junctions, particularly in the fourth exon, are defective in all species except chimp and human. Therefore, this isoform is most likely human or human/chimp specific and unlikely to play a role in a complex as highly conserved as the CSN.

A striking one-to-one correspondence exists between the CSN subunits, and those of the 19S lid subcomplex of the 26S proteasome, suggesting that they diversified from a common ancestor (Glickman et al., 1998; Seeger et al., 1998). The two signature structural motifs entail six subunits with a PCI and two with an MPN domain, all found within each of the complexes. The lid subunit DSS1 (Sem1 in budding yeast) is the only exception: DSS1 does not contain a PCI or MPN fold; moreover, it is missing a counterpart within the CSN. Considering that (1) like CSNAP, DSS1 links 19S proteasome lid subunits (Paraskevopoulos et al., 2014; Sone et al., 2004; Tomko and Hochstrasser, 2014), though an intact complex can be formed in its absence (Paraskevopoulos et al., 2014); (2) CSNAP and DSS1 are remarkably small proteins that share 18% sequential identity and 26% similarity, including a C-terminal region enriched with aromatic and acidic residues (Figure S4A); and (3) both proteins belong to the intrinsically unstructured protein family (Figure S4B), we suggest that DSS1 and CSNAP are paralogous subunits, filling the missing gap of homology between the 19S lid and CSN complexes (Figure 7).

Two decades have passed since the discovery of the CSN complex (Chamovitz et al., 1996; Wei et al., 1994); thus, a key question arises: How has the CSNAP/CSN association escaped previous detection? The answer probably lies within the sequence of CSNAP. First, the low molecular weight of the protein is likely to cause its rapid migration outside polyacrylamide electrophoresis gels, preventing its detection. Second, even if CSNAP is retained within the gel, the fact that it contains only two basic amino acids, i.e., two lysine residues, gives rise to poor Coomassie dye staining (Syrový and Hodný, 1991). Finally, proteomic identification of CSNAP might also be challenging, considering that tryptic peptides are typically analyzed (Mann et al., 2001). This procedure generates only two CSNAP peptides, and their long length, which is in the upper mass scale for typical analysis, also challenges identification. Hence, the methodology we described herein, which couples bottom-up and top-down MS analysis, set the stage for the discovery of CSNAP and paves the way toward identification of additional small proteins that act as integral subunits of large protein complexes.

## EXPERIMENTAL PROCEDURES

### Purification of the CSN Complex

CSN was isolated from human erythrocytes according to a previously published protocol (Hetfeld et al., 2005). FLAG purification of CSN is described in the Supplemental Experimental Procedures.

### Generation of a Polyclonal Antibody against CSNAP

The full-length CSNAP peptide was conjugated to KLH (Sigma Aldrich) using the $BS^3$ crosslinker (Pierce, Thermo Scientific) and used for immunization in rabbits. After three boosts, serum was obtained, and anti-CSNAP antibodies were affinity-purified on CSNAP peptide coupled to Aminolink beads (Pierce, Thermo Scientific) and stored in 50% glycerol at −20°C. Specificity was validated in comparison to pre-immune serum against synthetic CSNAP and cell lysates.

### Subcellular Fractionation

HeLa cells were fractionated to cytoplasmic, nuclear-soluble, and chromatin-bound fractions, with or without exposure to 20 $J/cm^2$ UV-C, as described previously (Füzesi-Levi et al., 2014). UV-C-exposed samples were collected 10 min after induction of UV damage.

### Activity Assay

Deneddylation activity of HAP1 cell lines was measured as in Füzesi-Levi et al. (2014). At each time point, deneddylation activity was calculated as the measured intensity of the deneddylated band divided by the total intensities of the neddylated and deneddylated bands and normalized to maximal activity (10 min). Average activity levels and SEs were calculated for each time point from three independent experiments.

### LC-MS Approach

The monolithic-LC-MS approach was performed as previously described (Rozen et al., 2013).

### Native MS Analysis

Nanoelectrospray ionization MS and MS/MS experiments were performed on a Synapt G2 instrument (Waters), as described previously (Kirshenbaum et al., 2010).

### Confocal Fluorescence Microscopy

Confocal fluorescence imaging and FRAP measurements were performed as previously described (Füzesi-Levi et al., 2014).

## SUPPLEMENTAL INFORMATION

Supplemental information includes Supplemental Experimental Procedures, seven figures, and two tables and can be found with this article online at http://dx.doi.org/10.1016/j.celrep.2015.09.021.

## AUTHOR CONTRIBUTIONS

S.R., G.B.-N., M.G.F.-L., and M.S. designed the experiments and analyzed the data. S.R., G.B.-N., M.G.F.-L. and L.M. performed the experiments. A.G., and Y.L. performed the absolute protein quantification. M.E. and S.B.-D. did the structural and bioinformatics analyses, respectively. S.R., G.B.-N., and M.S. wrote the manuscript.

## ACKNOWLEDGMENTS

We are grateful to Eitan Reuveny, Ning Wei, Yosef Shaul, and Haim Garty for providing plasmids and cells. We are thankful for the support of a Starting Grant from the European Research Council (ERC) (Horizon 2020)/ERC Grant Agreement no. 636752, an Acceleration Grant from the Israel Cancer Research Foundation, a Minerva Foundation grant, with funding from the Federal Ministry for Education and Research (Germany), and a grant from the Abisch-Frenkel Foundation (Switzerland). M.S. is the incumbent of the Elaine Blond Career Development Chair.

Received: April 16, 2015
Revised: August 4, 2015
Accepted: September 8, 2015
Published: October 8, 2015

## REFERENCES

Adler, A.S., Lin, M., Horlings, H., Nuyten, D.S., van de Vijver, M.J., and Chang, H.Y. (2006). Genetic regulators of large-scale transcriptional signatures in cancer. Nat. Genet. *38*, 421–430.

Adler, A.S., Littlepage, L.E., Lin, M., Kawahara, T.L., Wong, D.J., Werb, Z., and Chang, H.Y. (2008). CSN5 isopeptidase activity links COP9 signalosome activation to breast cancer progression. Cancer Res. *68*, 506–515.

Aravind, L., and Ponting, C.P. (1998). Homologues of 26S proteasome subunits are regulators of transcription and translation. Protein Sci. *7*, 1250–1254.

Beck, F., Unverdorben, P., Bohn, S., Schweitzer, A., Pfeifer, G., Sakata, E., Nickell, S., Plitzko, J.M., Villa, E., Baumeister, W., and Förster, F. (2012). Near-atomic resolution structural model of the yeast 26S proteasome. Proc. Natl. Acad. Sci. USA *109*, 14870–14875.

Ben-Shimon, A., and Eisenstein, M. (2010). Computational mapping of anchoring spots on protein surfaces. J. Mol. Biol. *402*, 259–277.

Bohn, S., Sakata, E., Beck, F., Pathare, G.R., Schnitger, J., Nágy, I., Baumeister, W., and Förster, F. (2013). Localization of the regulatory particle subunit Sem1 in the 26S proteasome. Biochem. Biophys. Res. Commun. *435*, 250–254.

Chamovitz, D.A., Wei, N., Osterlund, M.T., von Arnim, A.G., Staub, J.M., Matsui, M., and Deng, X.W. (1996). The COP9 complex, a novel multisubunit nuclear regulator involved in light control of a plant developmental switch. Cell *86*, 115–121.

Chen, J., Shin, J.H., Zhao, R., Phan, L., Wang, H., Xue, Y., Post, S.M., Ho Choi, H., Chen, J.S., Wang, E., et al. (2014). CSN6 drives carcinogenesis by positively regulating Myc stability. Nat. Commun. *5*, 5384.

Cope, G.A., Suh, G.S., Aravind, L., Schwarz, S.E., Zipursky, S.L., Koonin, E.V., and Deshaies, R.J. (2002). Role of predicted metalloprotease motif of Jab1/Csn5 in cleavage of Nedd8 from Cul1. Science *298*, 608–611.

da Fonseca, P.C., He, J., and Morris, E.P. (2012). Molecular model of the human 26S proteasome. Mol. Cell *46*, 54–66.

Deshaies, R.J., and Joazeiro, C.A. (2009). RING domain E3 ubiquitin ligases. Annu. Rev. Biochem. *78*, 399–434.

Drexler, H.G., Dirks, W.G., and MacLeod, R.A. (1999). False human hematopoietic cell lines: cross-contaminations and misinterpretations. Leukemia *13*, 1601–1607.

Dross, N., Spriet, C., Zwerger, M., Müller, G., Waldeck, W., and Langowski, J. (2009). Mapping eGFP oligomer mobility in living cell nuclei. PLoS ONE *4*, e5041.

Dunham, W.H., Larsen, B., Tate, S., Badillo, B.G., Goudreault, M., Tehami, Y., Kislinger, T., and Gingras, A.C. (2011). A cost-benefit analysis of multidimensional fractionation of affinity purification-mass spectrometry samples. Proteomics *11*, 2603–2612.

Dyson, H.J., and Wright, P.E. (2005). Intrinsically unstructured proteins and their functions. Nat. Rev. Mol. Cell Biol. *6*, 197–208.

Ebina, M., Tsuruta, F., Katoh, M.C., Kigoshi, Y., Someya, A., and Chiba, T. (2013). Myeloma overexpressed 2 (Myeov2) regulates L11 subnuclear localization through Nedd8 modification. PLoS ONE *8*, e65285.

Eisen, M.B., Spellman, P.T., Brown, P.O., and Botstein, D. (1998). Cluster analysis and display of genome-wide expression patterns. Proc. Natl. Acad. Sci. USA *95*, 14863–14868.

Ellisdon, A.M., Dimitrova, L., Hurt, E., and Stewart, M. (2012). Structural basis for the assembly and nucleic acid binding of the TREX-2 transcription-export complex. Nat. Struct. Mol. Biol. *19*, 328–336.

Emberley, E.D., Mosadeghi, R., and Deshaies, R.J. (2012). Deconjugation of Nedd8 from Cul1 is directly regulated by Skp1-F-box and substrate, and the COP9 signalosome inhibits deneddylated SCF by a noncatalytic mechanism. J. Biol. Chem. *287*, 29679–29689.

Enchev, R.I., Scott, D.C., da Fonseca, P.C., Schreiber, A., Monda, J.K., Schulman, B.A., Peter, M., and Morris, E.P. (2012). Structural basis for a reciprocal regulation between SCF and CSN. Cell Rep. *2*, 616–627.

Errington, W.J., Khan, M.Q., Bueler, S.A., Rubinstein, J.L., Chakrabartty, A., and Privé, G.G. (2012). Adaptor protein self-assembly drives the control of a cullin-RING ubiquitin ligase. Structure *20*, 1141–1153.

Fischer, E.S., Scrima, A., Böhm, K., Matsumoto, S., Lingaraju, G.M., Faty, M., Yasuda, T., Cavadini, S., Wakasugi, M., Hanaoka, F., et al. (2011). The molecular basis of CRL4DDB2/CSA ubiquitin ligase architecture, targeting, and activation. Cell *147*, 1024–1039.

Fukunaga, K., Kudo, T., Toh-e, A., Tanaka, K., and Saeki, Y. (2010). Dissection of the assembly pathway of the proteasome lid in Saccharomyces cerevisiae. Biochem. Biophys. Res. Commun. *396*, 1048–1053.

Füzesi-Levi, M.G., Ben-Nissan, G., Bianchi, E., Zhou, H., Deery, M.J., Lilley, K.S., Levin, Y., and Sharon, M. (2014). Dynamic regulation of the COP9 signalosome in response to DNA damage. Mol. Cell. Biol. *34*, 1066–1076.

Glickman, M.H., Rubin, D.M., Coux, O., Wefes, I., Pfeifer, G., Cjeka, Z., Baumeister, W., Fried, V.A., and Finley, D. (1998). A subcomplex of the proteasome regulatory particle required for ubiquitin-conjugate degradation and related to the COP9-signalosome and eIF3. Cell *94*, 615–623.

Groisman, R., Polanowska, J., Kuraoka, I., Sawada, J., Saijo, M., Drapkin, R., Kisselev, A.F., Tanaka, K., and Nakatani, Y. (2003). The ubiquitin ligase activity in the DDB2 and CSA complexes is differentially regulated by the COP9 signalosome in response to DNA damage. Cell *113*, 357–367.

Hetfeld, B.K., Bech-Otschir, D., and Dubiel, W. (2005). Purification method of the COP9 signalosome from human erythrocytes. Methods Enzymol. *398*, 481–491.

Hofmann, K., and Bucher, P. (1998). The PCI domain: a common theme in three multiprotein complexes. Trends Biochem. Sci. *23*, 204–205.

Jansen, R., Greenbaum, D., and Gerstein, M. (2002). Relating whole-genome expression data with protein-protein interactions. Genome Res. *12*, 37–46.

Kalkhof, S., and Sinz, A. (2008). Chances and pitfalls of chemical cross-linking with amine-reactive N-hydroxysuccinimide esters. Anal. Bioanal. Chem. *392*, 305–312.

Kao, A., Randall, A., Yang, Y., Patel, V.R., Kandur, W., Guan, S., Rychnovsky, S.D., Baldi, P., and Huang, L. (2012). Mapping the structural topology of the yeast 19S proteasomal regulatory particle using chemical cross-linking and probabilistic modeling. Mol. Cell. Proteomics *11*, 1566–1577.

Kirshenbaum, N., Michaelevski, I., and Sharon, M. (2010). Analyzing large protein complexes by structural mass spectrometry. J. Vis. Exp. (*40*), 1954.

Lander, G.C., Estrin, E., Matyskiela, M.E., Bashore, C., Nogales, E., and Martin, A. (2012). Complete subunit architecture of the proteasome regulatory particle. Nature *482*, 186–191.

Lasker, K., Förster, F., Bohn, S., Walzthoeni, T., Villa, E., Unverdorben, P., Beck, F., Aebersold, R., Sali, A., and Baumeister, W. (2012). Molecular architecture of the 26S proteasome holocomplex determined by an integrative approach. Proc. Natl. Acad. Sci. USA *109*, 1380–1387.

Lee, M.H., Zhao, R., Phan, L., and Yeung, S.C. (2011). Roles of COP9 signalosome in cancer. Cell Cycle *10*, 3057–3066.

Lingaraju, G.M., Bunker, R.D., Cavadini, S., Hess, D., Hassiepen, U., Renatus, M., Fischer, E.S., and Thomä, N.H. (2014). Crystal structure of the human COP9 signalosome. Nature *512*, 161–165.

Luijsterburg, M.S., Goedhart, J., Moser, J., Kool, H., Geverts, B., Houtsmuller, A.B., Mullenders, L.H., Vermeulen, W., and van Driel, R. (2007). Dynamic in vivo interaction of DDB2 E3 ubiquitin ligase with UV-damaged DNA is independent of damage-recognition protein XPC. J. Cell Sci. *120*, 2706–2716.

Lydeard, J.R., Schulman, B.A., and Harper, J.W. (2013). Building and remodelling Cullin-RING E3 ubiquitin ligases. EMBO Rep. *14*, 1050–1061.

Mann, M., Hendrickson, R.C., and Pandey, A. (2001). Analysis of proteins and proteomes by mass spectrometry. Annu. Rev. Biochem. *70*, 437–473.

Maytal-Kivity, V., Pick, E., Piran, R., Hofmann, K., and Glickman, M.H. (2003). The COP9 signalosome-like complex in S. cerevisiae and links to other PCI complexes. Int. J. Biochem. Cell Biol. *35*, 706–715.

Ménétret, J.F., Schaletzky, J., Clemons, W.M., Jr., Osborne, A.R., Skånland, S.S., Denison, C., Gygi, S.P., Kirkpatrick, D.S., Park, E., Ludtke, S.J., et al. (2007). Ribosome binding of a single copy of the SecY complex: implications for protein translocation. Mol. Cell *28*, 1083–1092.

Moreno-Hagelsieb, G., Treviño, V., Pérez-Rueda, E., Smith, T.F., and Collado-Vides, J. (2001). Transcription unit conservation in the three domains of life: a perspective from Escherichia coli. Trends Genet. *17*, 175–177.

Nakasone, A., Fujiwara, M., Fukao, Y., Biswas, K.K., Rahman, A., Kawai-Yamada, M., Narumi, I., Uchimiya, H., and Oono, Y. (2012). SMALL ACIDIC PROTEIN1 acts with RUB modification components, the COP9 signalosome, and AXR1 to regulate growth and development of Arabidopsis. Plant Physiol. *160*, 93–105.

Olma, M.H., Roy, M., Le Bihan, T., Sumara, I., Maerki, S., Larsen, B., Quadroni, M., Peter, M., Tyers, M., and Pintard, L. (2009). An interaction network of the mammalian COP9 signalosome identifies Dda1 as a core subunit of multiple Cul4-based E3 ligases. J. Cell Sci. *122*, 1035–1044.

Paraskevopoulos, K., Kriegenburg, F., Tatham, M.H., Rösner, H.I., Medina, B., Larsen, I.B., Brandstrup, R., Hardwick, K.G., Hay, R.T., Kragelund, B.B., et al. (2014). Dss1 is a 26S proteasome ubiquitin receptor. Mol. Cell *56*, 453–461.

Rahman, A., Nakasone, A., Chhun, T., Ooura, C., Biswas, K.K., Uchimiya, H., Tsurumi, S., Baskin, T.I., Tanaka, A., and Oono, Y. (2006). A small acidic protein 1 (SMAP1) mediates responses of the Arabidopsis root to the synthetic auxin 2,4-dichlorophenoxyacetic acid. Plant J. *47*, 788–801.

Richardson, K.S., and Zundel, W. (2005). The emerging role of the COP9 signalosome in cancer. Mol. Cancer Res. *3*, 645–653.

Rockel, B., Schmaler, T., Huang, X., and Dubiel, W. (2014). Electron microscopy and in vitro deneddylation reveal similar architectures and biochemistry of isolated human and Flag-mouse COP9 signalosome complexes. Biochem. Biophys. Res. Commun. *450*, 991–997.

Rozen, S., Tieri, A., Ridner, G., Stark, A.K., Schmaler, T., Ben-Nissan, G., Dubiel, W., and Sharon, M. (2013). Exposing the subunit diversity within protein complexes: a mass spectrometry approach. Methods *59*, 270–277.

Scheel, H., and Hofmann, K. (2005). Prediction of a common structural scaffold for proteasome lid, COP9-signalosome and eIF3 complexes. BMC Bioinformatics *6*, 71.

Schwechheimer, C. (2004). The COP9 signalosome (CSN): an evolutionary conserved proteolysis regulator in eukaryotic development. Biochim. Biophys. Acta *1695*, 45–54.

Seeger, M., Kraft, R., Ferrell, K., Bech-Otschir, D., Dumdey, R., Schade, R., Gordon, C., Naumann, M., and Dubiel, W. (1998). A novel protein complex involved in signal transduction possessing similarities to 26S proteasome subunits. FASEB J. *12*, 469–478.

Sharon, M. (2013). Biochemistry. Structural MS pulls its weight. Science *340*, 1059–1060.

Sharon, M., Taverner, T., Ambroggio, X.I., Deshaies, R.J., and Robinson, C.V. (2006). Structural organization of the 19S proteasome lid: insights from MS of intact complexes. PLoS Biol. *4*, e267.

Sone, T., Saeki, Y., Toh-e, A., and Yokosawa, H. (2004). Sem1p is a novel subunit of the 26 S proteasome from Saccharomyces cerevisiae. J. Biol. Chem. *279*, 28807–28816.

Soucy, T.A., Smith, P.G., Milhollen, M.A., Berger, A.J., Gavin, J.M., Adhikari, S., Brownell, J.E., Burke, K.E., Cardin, D.P., Critchley, S., et al. (2009). An inhibitor of NEDD8-activating enzyme as a new approach to treat cancer. Nature *458*, 732–736.

Sowa, M.E., Bennett, E.J., Gygi, S.P., and Harper, J.W. (2009). Defining the human deubiquitinating enzyme interaction landscape. Cell *138*, 389–403.

Syrový, I., and Hodný, Z. (1991). Staining and quantification of proteins separated by polyacrylamide gel electrophoresis. J. Chromatogr. A *569*, 175–196.

Tang, L.J., Hu, W.X., He, L.F., Tian, J.Y., Liu, X.F., and Tan, D.R. (2003). Molecular cloning and analysis of a novel gene over-expressed in multiple myeloma cells. Chin. J. Biochem. Mol. Biol. *19*, 60–63.

Tomko, R.J., Jr., and Hochstrasser, M. (2014). The intrinsically disordered Sem1 protein functions as a molecular tether during proteasome lid biogenesis. Mol. Cell *53*, 433–443.

Wei, N., Chamovitz, D.A., and Deng, X.W. (1994). Arabidopsis COP9 is a component of a novel signaling complex mediating light control of development. Cell *78*, 117–124.

Wei, N., Serino, G., and Deng, X.W. (2008). The COP9 signalosome: more than a protease. Trends Biochem. Sci. *33*, 592–600.

Yang, H., Jeffrey, P.D., Miller, J., Kinnucan, E., Sun, Y., Thoma, N.H., Zheng, N., Chen, P.L., Lee, W.H., and Pavletich, N.P. (2002). BRCA2 function in DNA binding and recombination from a BRCA2-DSS1-ssDNA structure. Science *297*, 1837–1848.

Zhang, S.N., Pei, D.S., and Zheng, J.N. (2013). The COP9 signalosome subunit 6 (CSN6): a potential oncogene. Cell Div. *8*, 14.

Zhuang, M., Calabrese, M.F., Liu, J., Waddell, M.B., Nourse, A., Hammel, M., Miller, D.J., Walden, H., Duda, D.M., Seyedin, S.N., et al. (2009). Structures of SPOP-substrate complexes: insights into molecular architectures of BTB-Cul3 ubiquitin ligases. Mol. Cell *36*, 39–50.